

# High-speed device-independent quantum key distribution against collective attacks

Wen-Zhao Liu,<sup>1, 2, 3</sup> Yu-Zhe Zhang,<sup>1, 2, 3</sup> Yi-Zheng Zhen,<sup>1, 2, 3</sup> Ming-Han Li,<sup>1, 2, 3</sup> Yang Liu,<sup>1, 2, 3</sup> Jingyun Fan,<sup>4</sup> Feihu Xu,<sup>1, 2, 3</sup> Qiang Zhang,<sup>1, 2, 3</sup> and Jian-Wei Pan<sup>1, 2, 3</sup>

<sup>1</sup>*Hefei National Laboratory for Physical Sciences at Microscale and Department of Modern Physics, University of Science and Technology of China, Hefei 230026, P. R. China.*

<sup>2</sup>*Shanghai Branch, CAS Center for Excellence and Synergetic Innovation Center in Quantum Information and Quantum Physics, University of Science and Technology of China, Shanghai 201315, P. R. China.*

<sup>3</sup>*Shanghai Research Center for Quantum Sciences, Shanghai 201315, P. R. China.*

<sup>4</sup>*Shenzhen Institute for Quantum Science and Engineering and Department of Physics, Southern University of Science and Technology, Shenzhen, 518055, P. R. China*

The security of quantum key distribution (QKD) [1, 2] usually relies on that the users's devices are well characterized according to the security models made in the security proofs [3]. In contrast, device-independent QKD [4–11] — an entanglement-based protocol [2] — permits the security even without any knowledge of the underlying devices. Despite its beauty in theory, device-independent QKD is elusive to realize with current technology. This is because a faithful realization requires a high-quality violation of Bell inequality without the fair-sampling assumption [12, 13]. Particularly, in a photonic realization, a rather high detection efficiency is needed where the threshold values depend on the security proofs [7–11]; this efficiency is far beyond the current reach [12–24]. Here, both theoretical and experimental innovations yield the realization of device-independent QKD based on a photonic setup. On the theory side, to relax the threshold efficiency for practical device-independent QKD, we exploit the random post-selection [25] combined with adding noise [26] for preprocessing, and compute the entropy with complete nonlocal correlations [27]. On the experiment side, we develop a high-quality polarization-entangled photonic source and achieve state-of-the-art (heralded) detection efficiency of 87.49%, which outperforms previous experiments [12–24] and satisfies the threshold efficiency for the first time. Together, we demonstrate device-independent QKD at a secret key rate of 466 bits/s over 20 m standard fiber in the asymptotic limit against collective attacks. Besides, we show the feasibility of generating secret keys at a fiber length of 220 meters. Importantly, our photonic implementation can generate entangled photons at a high rate and in the telecom wavelength, which is desirable for high-speed key generation over long distances. The results not only prove the feasibility of device-independent QKD with realistic devices, but also push the security of communication to an unprecedented level.

*Introduction.* — Quantum key distribution (QKD) [1, 2] allows two distant users to share a secret key with information-theoretical security [3]. The security of QKD usually relies on the assumption that the devices are trusted and well-characterized [28–30]. In practice, however, the imperfections in realistic devices may introduce potential backdoors or side channels [31, 32]. Measurement-device-independent QKD [33, 34] (see also an efficient version [35]) was proposed to remove the side channels in measurement settings, but its state-preparation devices have to be precisely calibrated. Notably, device-independent QKD [4–7] relaxes conventional security assumption on the devices. With minimal assumptions satisfied [7], e.g., the devices have no memory between trials [36, 37] and the classical processing units are trusted, the security of device-independent QKD can be guaranteed based solely on the violation of a Bell inequality.

Device-independent QKD is not an easy task with current technology. A realization typically requires that a Bell inequality is violated in a loophole-free fashion [38, 39]. A key problem in the photonic implementation is the limited detection efficiency, e.g., the emitted photons in experiments may not be detected due to the losses in the transmission or the imperfect detectors. Al-

though researchers have closed the detection loopholes in recent experiments with efficiency  $\eta \sim 80\%$  [12–24], a much higher efficiency, e.g.,  $\eta > 90\%$ , is normally required for the purpose of device-independent QKD [7–11]. Despite recent theory progress [26, 27, 40–46], a practical implementation of device-independent QKD remains elusive.

Here we report the first experimental realization of device-independent QKD with entangled photons, thanks to the significant advancements at both theoretical and experimental sides. On the theoretical side, we propose a protocol to greatly enhance the loss tolerance in the practical case of device imperfections which requires a single-photon system efficiency of about 86%, and provide a security proof against collective attacks (see the Appendix for details). The basic idea of our protocol is to extract secret keys in the post-selected strings of outcomes [25, 47] and then add the noise [26] to the survived raw keys, where the lower bound of quantum conditional entropy can be computed based on the framework in ref. [27]. On the experimental side, we achieve a single-photon system efficiency of greater than 87% which surpasses the values reported in previous loophole free Bell test experiments with photons [12–24] (see Table II). Combining the experimental and theoretical

advances, we present a proof-of-principle experimental demonstration of device-independent QKD over standard fiber distances up to 220 meters.

*Protocol.* Our protocol is constructed based on a Bell test. As shown in Fig. 3, a pair of entangled photons are shared between Alice and Bob. We consider the scenario that Alice’s measurement has binary input  $x \in \{1, 2\}$  and binary outcome  $a$  and Bob’s measurement has triple input  $y \in \{1, 2, 3\}$  and binary outcome  $b$ , where  $a, b = 0(1)$  if the respective detector does (not) register an event, i.e. “click” (or “no-click”). We denote the probability of joint measurement with outcomes  $(a, b)$  conditioning upon the measurement inputs  $(x, y)$  as  $P(a, b|x, y)$ .

Modified after Ref. [7], our device-independent QKD protocol is readily to be implemented in the state-of-art quantum optical experiments with the addition of new features, which are briefly summarized here (see the Appendix for details). Consider  $N$ –rounds of Bell test experiment described in Fig. 3, we randomly select a round of experiment whose measurement inputs are  $(\bar{x}, \bar{y}) = (1, 3)$  as “key-generation rounds” and use the unselected rounds of experiments as “test rounds” to test nonlocal correlation. For the selected “key-generation rounds” of experiments, Alice and Bob each randomly and independently keep (or discard) a round of experiment with probability  $p$  (or  $1 - p$ ) if the respective measurement outcome is a “non-click” and keep a round of experiment if the respective outcome is a “click”. After this post-selection procedure, both Alice and Bob announce the discarded rounds using an authenticated public channel. Those “key-generation rounds” of experiments which are not kept by Alice and Bob simultaneously are discarded. Then, Alice further performs a noisy preprocessing. She generates the noisy raw keys  $\hat{a}_{\bar{x}}$  by flipping each of her survived key bits independently with probability  $p_N$ . The protocol is then proceeded with an error correction step that allows Bob to infer Alice’s new (noisy) raw key. The final secret key can be obtained after the privacy amplification. We compile an experimental procedure of our protocol which is listed in Table I.

We remark that the random post selection can effectively remove the no-detection events that contain little correlations but high errors, which can effectively reduce the information cost of error correction [25]. The noisy preprocessing can decrease the correlation between Alice and Eve by mixing the probability distributions with randomness [26]. These two additional processing steps can effectively facilitate the enhancement of loss tolerance (See the Appendix for details).

*Key rate from the preprocessed events.* We consider the collective attack model [7] where the devices behave in an independent and identically distributed (i.i.d.) manner and the devices are memoryless [36, 37] at each step of the protocol. For the process of random post-selection, let  $p_\alpha = 1 \cdot \delta_{\alpha,0} + p \cdot \delta_{\alpha,1}$  such that a given event  $(a, b)$  can be kept with probability  $\omega_{ab} = p_a \cdot p_b$ . Suppose that for a given “key-generation round”, the probability that

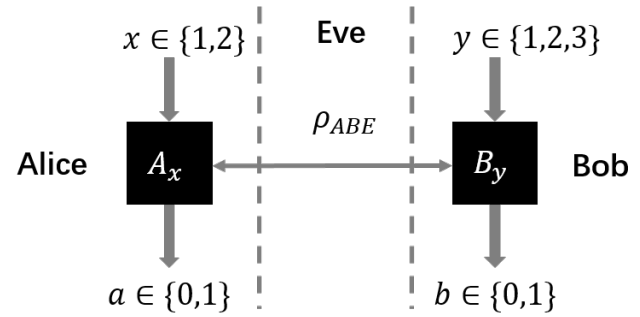


FIG. 1. An illustration of the device-independent QKD protocol. Alice and Bob share a pair of entangled photons potentially controlled by Eve ( $\rho_{ABE}$ ). Alice performs a measurement to her share with binary input  $x \in \{1, 2\}$  and binary output  $a \in \{0, 1\}$ . Bob performs a measurement to his share with triple input  $y \in \{1, 2, 3\}$  and binary output  $b \in \{0, 1\}$ .

TABLE I. The device-independent QKD protocol with preprocessing.

**Assumptions** [7]: We focus on collective attacks and assume that the devices are memoryless and behave identically and independently at each step of the protocol.

**Distribution:** A source, potentially controlled by Eve, distributes entangled photons to Alice and Bob.

**Measurements:** Alice and Bob randomly choose measurement settings  $x \in \{1, 2\}$  and  $y \in \{1, 2, 3\}$  to measure their own part, respectively.

**Form the raw keys:** They use a fraction of strings corresponding to  $(\bar{x}, \bar{y}) = (1, 3)$  as the “key-generation round” to generate the raw keys, while all the other strings are used as the “test round” to characterize the nonlocal correlations.

**Random post-selection** [25]: For the “key-generation round”, Alice and Bob each randomly and independently discards the non-click bits with probability  $1 - p$ , while they keep all the click bits.

**Noisy preprocessing** [26]: Alice generates the noisy raw keys  $\hat{a}_{\bar{x}}$  by flipping each of her survived key bits independently with probability  $p_N$ .

**Error correction and Privacy amplification:** A secret key is distilled asymptotically via a one-way error correction protocol and a privacy amplification procedure.

it can be kept is  $p_{\mathcal{V}_p} = \sum_{ab \in \mathcal{V}} \omega_{ab} P(a, b|\bar{x}, \bar{y})$ , where  $\mathcal{V}_p$  represents the set of post-selected events. In the limit of infinite data size, for a given set of bipartite correlations  $\{P(a, b|x, y)\}$  that characterize the devices, the secret key rate  $r$  with optimal error correction can be lower-bounded by the Devetak-Winter rate [48],

$$r \geq p_{\mathcal{V}_p} \left[ H(\hat{A}_{\bar{x}}|E, \mathcal{V}_p) - H(\hat{A}_{\bar{x}}|B_{\bar{y}}, \mathcal{V}_p) \right], \quad (1)$$

where  $H(\hat{A}_{\bar{x}}|E, \mathcal{V}_p)$  is the single-run conditional von Neu-

mann entropy that quantifies the strength of the correlations between Alice and Eve. We here use  $\hat{A}_{\bar{x}}$  represent the final key bits of Alice after the step of random post-selection and noisy preprocessing.  $H(\hat{A}_{\bar{x}}|B_{\bar{y}}, \mathcal{V}_p)$  is the single-run cost of one-way error correction from Alice to Bob.  $p_{\mathcal{V}_p}$  represents survived probability of the single-run pair of key bits. We adopt the method in Ref. [27] to show that the single-run conditional von Neumann entropy  $H(\hat{A}_{\bar{x}}|E, \mathcal{V}_p)$  can be bounded by a converging sequence of optimizations that can be subsequently computed using the NPA hierarchy [49] (see the Appendix for details). Note that for the “test round”, Alice and Bob keep all the outcomes without any post-selection such that the Bell test is done without detection loopholes [47].

TABLE II. Efficiencies in existing photonic experiments of *loophole-free* Bell tests and related applications. The efficiencies in the table are averaged over Alice’s and Bob’s global detection efficiency. (QRNG: quantum random number generation)

Label	Experiment	Year	Type	Efficiency
(1)	Shalm <i>et al.</i> [14]	2015	Bell test	75.15%
(2)	Giustina <i>et al.</i> [15]	2015	Bell test	77.40%
(3)	Liu <i>et al.</i> [17]	2018	QRNG	79.40%
(4)	Shen <i>et al.</i> [18]	2018	QRNG	82.33%
(5)	Bierhorst <i>et al.</i> [19]	2018	QRNG	75.50%
(6)	Liu <i>et al.</i> [20]	2018	QRNG	78.65%
(7)	Li <i>et al.</i> [16]	2018	Bell test	78.75%
(8)	Zhang <i>et al.</i> [21]	2020	QRNG	76.00%
(9)	Shalm <i>et al.</i> [24]	2021	QRNG	76.30%
(10)	Li <i>et al.</i> [23]	2021	QRNG	81.35%
(11)	Liu <i>et al.</i> [22]	2021	QRNG	84.10%
(12)	This work	2021	QKD	87.49%

*Experiment.* — A schematic of the experiment is depicted in Fig. 2 which consists of three modules. Pairs of polarization-entangled photons at the wavelength of 1560 nm are generated probabilistically via the spontaneous parametric downconversion process in the central module (a). The pairs of photons are sent to two side modules (b), where Alice and Bob perform correlated detections to generate secret keys. The single-photon detection efficiency is respectively determined to be  $87.16 \pm 0.22\%$  and  $87.82 \pm 0.21\%$  for Alice and Bob (see the Appendix for details), which significantly surpass the record values in previous loophole-free Bell tests with photons [14–24] (see Table II). Furthermore, the values also surpass the efficiency threshold of 86.2% for device-independent key generation in a realistic scenario.

According to the numerical studies, we prepare a non-maximally two-photon entangled state  $\cos(20.0^\circ)|HV\rangle + \sin(20.0^\circ)|VH\rangle$  and set the measurement settings to  $\{-88.22^\circ, 54.29^\circ\}$  and  $\{9.75^\circ, 21.45^\circ, -1.07^\circ\}$  respectively for  $x \in \{1, 2\}$  and  $y \in \{1, 2, 3\}$  to optimize the probability of key generation, where the values presented in degree are angles of half-wave plates in the polarization measurements by Alice and Bob (Fig. 2). We experimen-

tally measure a two-photon state fidelity of  $99.52 \pm 0.15\%$  with respect to the ideal state and achieve a CHSH game winning probability of 0.7559, both substantially improving over previous results [16, 17, 20, 22, 23] (see the Appendix for details). We repeat the experiment at a rate of  $2 \times 10^6$  rounds per second.

In this proof-of-principle experimental demonstration, we place Alice and Bob in the same lab with a distance of 20 meters (mainly the fiber length). We have adopted the shielding assumption [22, 50] to prohibit unnecessary communications between relevant events taking place in three modules and between these events and adversaries. We alternate the measurement settings instead of randomization to reduce experimental complexity.

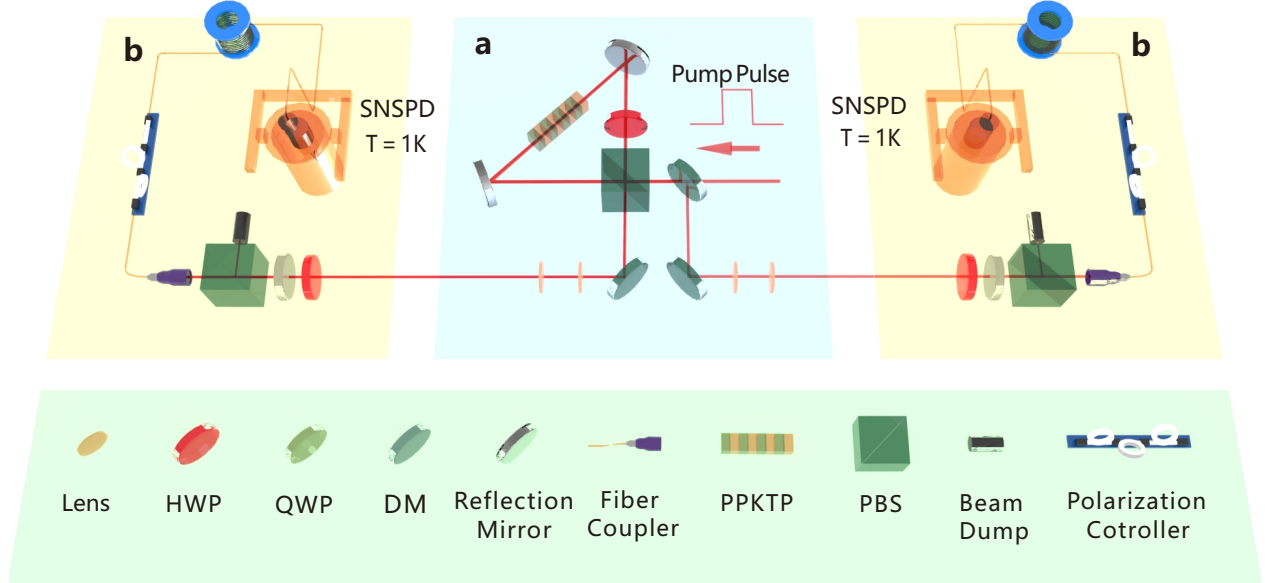
We conduct  $2.4 \times 10^8$  rounds of experiment for each of the six combinations of measurement settings  $(x, y)$  and perform data analysis following the protocol. With optimized parameters  $p_N = 0.13$  and  $p = 0.96$ , we obtain  $H(\hat{A}_{\bar{x}}|E, \mathcal{V}_p) = 0.560206$  and  $H(\hat{A}_{\bar{x}}|B, \mathcal{V}_p) = 0.559953$ . (see the Appendix for details). Finally, according the asymptotic key rate in Eq. (1), 55,920 bits of secret keys are expected to be distilled after error correction and privacy amplification. This corresponds to  $2.33 \times 10^{-4}$  bit per round or 466 bits per second. Furthermore, we show the feasibility to successfully generate secret keys at a fiber length of 220 meters by conducting the same rounds of experiments, for which we re-optimize the experiment over  $p_N$  and  $p$ . These results are shown in Tab. III. This shows the loss tolerance of our system to conduct device-independent QKD at longer distances over telecom fiber.

TABLE III. The secret key rate as a function of the fiber distance between Alice and Bob. We test the device-independent QKD protocol by adding different length of fibers.

Fiber length/m	Key rate/ $\text{bit} \cdot \text{s}^{-1}$	$p_N$	$p$
20	466	0.13	0.96
80	107.4	0.17	0.94
220	2.6	0.49	0.99

*Conclusion.* — In conclusion, we have reported an experimental realization of device-independent QKD against collective attacks with a photonic setup. Our photonic implementation can generate entangled photons at a high rate and in the telecom wavelength, which is desirable for the practical applications. This photonic platform can be naturally combined with quantum memory and quantum repeaters to form a quantum internet. In future, by using the framework of entropy accumulation theorem [51], our protocol and security analysis can be extended to the consideration of finite-key effects [11]. Overall, the successful implementation of device-independent QKD paves the way for the further realizations and applications of quantum communication and quantum information processing in a device-independence manner.

*Note added.* When we are completing the manuscript, we notice two concurrent proof-of-concept device-



**FIG. 2. Schematic of the experiment.** **a** Entanglement Source, Creation of pairs of entangled photons: Light pulses of 10 ns are injected at a repetition pulse rate of 2 MHz into a periodically poled potassium titanyl phosphate (PPKTP) crystal in a Sagnac loop to generate polarization-entangled photon pairs. The two photons of an entangled pair at 1560 nm travel in opposite directions to two sites Alice and Bob, where they are subject to polarization projection measurements. we place the PPKTP at a small angle with the light path. This will not significantly affect the upper limit of efficiency that the system could achieve, but it could effectively reduce the reflection of the 1560 nm photons on the inner surface of the PPKTP crystal when the devices are not perfect. These enhancements lead that the non-maximally entangled state generated in our experiment has a better fidelity  $99.52 \pm 0.15\%$  as compared to our previous work [20, 22, 23]. **b** Alice and Bob, single-photon polarization measurement: In the measurement sites, Alice (Bob) uses a HWP to project the single photon into pre-determined measurement bases. After being collected into the fiber, the single photons transmit through a certain length of fiber and then are detected by a superconducting nanowire single-photon detector (SNSPD) operating at 1K. HWP – half-wave plate; QWP – quarter-wave plate; DM – dichroic mirror; PBS – polarizing beam splitter.

independent QKD experiments based on trapped ions [52] and trapped atoms [53]. In contrast to those systems, our photonic implementation can generate entangled photons at a high rate in the telecom wavelength, which is suitable for high-speed key generation over long-haul optical fiber networks.

#### ACKNOWLEDGMENTS

We thank Peter Brown, Roger Colbeck, Charles Lim, Nicolas Sangouard, Jean-Daniel Bancal, Yan-

bao Zhang, Xingjian Zhang for enlightening discussions. This work was supported by the National Key Research and Development (R&D) Plan of China (2018YFB0504300,2020YFA0309701), the National Natural Science Foundation of China (617714438,62031024), the Anhui Initiative in Quantum Information Technologies, the Chinese Academy of Sciences and the Key-Area Research and Development Program of Guangdong Province (2020B0303010001, 2019ZT08X324).

Wen-Zhao Liu and Yu-Zhe Zhang contribute equally.

#### Appendix A: Theoretical analysis

##### 1. Key rate from the post-selected events

Before we give the security proof, we first give a detailed description of our protocol. As shown in Fig. 3, the protocol we adopted is a modification of ref. [7] with a photonic realization. Alice and Bob share a quantum channel consisting of a source that emits entangled photon pairs. After receiving the photon, Alice (or Bob) randomly chooses a measurement setting  $x \in \{1, 2\}$  (or  $y \in \{1, 2, 3\}$ ) and measures her (or his) part. Denote the measurements as  $A_x$

and  $B_y$  for Alice's and Bob's measurements, respectively. For each input  $x$  and  $y$ , binary outcomes are observed by Alice and Bob: a click in the detector labeled as “0”, or a non-click labeled as “1”.

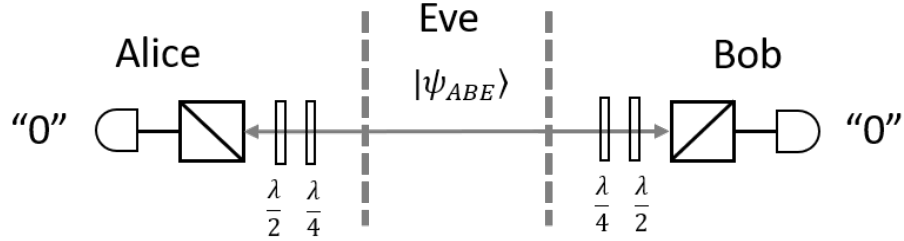


FIG. 3. An illustration of the device-independent QKD protocol used in this experiment. Entangled photon pairs are created by a source that is potentially controlled by Eve, and then they are distributed between Alice and Bob. Each of them performs measurements using a polarising beam-splitter (PBS) and a detector. A set of wave-plates  $\lambda/4, \lambda/2$  allows them to choose the measurement setting, i.e. the angle of polarisation. Each party effectively produces one of two possible outcomes, 0 for a click event and 1 for a non-click event.

We first drive the cq-state after the step of post selection and noisy preprocessing. Let  $Q_A$ ,  $Q_B$  and  $Q_E$  be the three Hilbert spaces corresponding to Alice's device, Bob's device and Eve's device, respectively. Since we focus on collective attacks and assume that the devices are memoryless and behave identically and independently at each step of the protocol, at the beginning of each round, a tripartite state  $\rho_{ABE}$  is shared among Alice, Bob, and Eve. After the measurements, the joint distribution of Alice's and Bob's outputs with respective to measurement settings can be described as

$$P(a, b|x, y) = \text{Tr}[(A_{a|x} \otimes B_{b|y} \otimes I)\rho_{ABE}]. \quad (\text{A1})$$

Here,  $A_{a|x}$  and  $B_{b|y}$  are the positive-operator-valued-measures associated with Alice's and Bob's measurement.

In our protocol, Alice/Bob randomly and independently post-selects her/his own outcomes “1” with respect to the key-generation rounds  $(\bar{x}, \bar{y})$ , such that a given event  $(a, b)$  can be kept with probability  $\omega_{ab} = p_a \cdot p_b$ , where  $p_a = 1 \cdot \delta_{a,0} + p \cdot \delta_{a,1}$ . Conditioned on the post-selected events  $\mathcal{V}_p$ , the quantum side information before noisy preprocessing can be represented by the state  $\rho_{\tilde{A}E|\mathcal{V}_p} = \frac{1}{p_{\mathcal{V}_p}} \sum_{ab \in \mathcal{V}} \omega_{ab} |ab\rangle\langle ab| \otimes \rho_{ab}^E$ , where  $\rho_{ab}^E = \text{Tr}_{AB}[(A_{a|\bar{x}} \otimes B_{b|\bar{y}} \otimes I)\rho_{ABE}]$ , and the probability distributions  $\tilde{\mathbf{P}}$  of the post-selected events in  $\mathcal{V}_p$  are thus given by,

$$\tilde{P}(a, b|\bar{x}, \bar{y}, \mathcal{V}_p) = P(a, b|\bar{x}, \bar{y}) \cdot \omega_{ab} / p_{\mathcal{V}_p}. \quad (\text{A2})$$

By taking the partial trace over  $Q_B$ , we have

$$\rho_{\tilde{A}E|\mathcal{V}_p} = \frac{1}{p_{\mathcal{V}_p}} [|0\rangle\langle 0| \otimes (\rho_{00}^E + p \cdot \rho_{01}^E) + |1\rangle\langle 1| \otimes (p \cdot \rho_{10}^E + p^2 \cdot \rho_{11}^E)]. \quad (\text{A3})$$

We remind that before the post-selection procedure, Eve couldn't get to know which runs are kept, since he should not have access to the outputs observed by the parties. After Alice and Bob announce the discarded rounds using an authenticated public channel, Eve would know exactly which run he should try to guess and is thus advantageous for him [47].

For the process of noisy preprocessing, Alice generates the noisy raw keys  $\hat{a}_{\bar{x}}$  by flipping each of her survived key bits independently with probability  $p_N$ . After noisy preprocessing, the final cq-state can be computed as

$$\begin{aligned} \rho_{\hat{A}E|\mathcal{V}_p} = \frac{1}{p_{\mathcal{V}_p}} & \{ |0\rangle\langle 0| \otimes [(1 - p_N) \cdot (\rho_{00}^E + p \cdot \rho_{01}^E) + p_N \cdot (p \cdot \rho_{10}^E + p^2 \cdot \rho_{11}^E)] \\ & + |1\rangle\langle 1| \otimes [(1 - p_N) \cdot (p \cdot \rho_{10}^E + p^2 \cdot \rho_{11}^E) + p_N \cdot (\rho_{00}^E + p \cdot \rho_{01}^E)] \}, \end{aligned} \quad (\text{A4})$$

with the final probability distribution  $\hat{P}(a, b|\bar{x}, \bar{y}, \mathcal{V}_p)$  in the set  $\mathcal{V}_p$ ,

$$\hat{P}(a, b|\bar{x}, \bar{y}, \mathcal{V}_p) = (1 - p_N) \tilde{P}(a, b|\bar{x}, \bar{y}, \mathcal{V}_p) + p_N \tilde{P}(a \oplus 1, b|\bar{x}, \bar{y}, \mathcal{V}_p). \quad (\text{A5})$$

Here, modulo 2 is denoted as  $\oplus$ . From Eq. A5, the cost of one-way error correction from Alice to Bob,  $H(\hat{A}_{\bar{x}}|B_{\bar{y}}, \mathcal{V}_p)$ , is supposed to be quantified by

$$H(\hat{A}_{\bar{x}}|B_{\bar{y}}, \mathcal{V}_p) = \sum_{a,b} h[\hat{P}(a, b|\bar{x}, \bar{y}, \mathcal{V}_p)] - \sum_b h[\hat{P}(0, b|\bar{x}, \bar{y}, \mathcal{V}_p) + \hat{P}(1, b|\bar{x}, \bar{y}, \mathcal{V}_p)], \quad (\text{A6})$$

where  $h(x)$  is defined by  $h(x) = -x \log_2 x$ .

To continue the security proof, our objective is to bound the quantum conditional entropy  $H(\hat{A}_{\bar{x}}|E, \mathcal{V}_p)$ . It quantifies the correlation between Alice and Eve, and hence the secrecy of the key. In the following subsection, we adopt the method in Ref. [27] to obtain a lower bound on  $H(\hat{A}_{\bar{x}}|E, \mathcal{V}_p)$ . To quantify the secret key, the non-local Bell test takes the the full statistics into account, which is potentially more efficient than the one based on violating specific Bell inequalities [47, 54, 55] and won't open the detection loophole [47].

## 2. Lower bounds on the conditional von Neumann entropy

In order to obtain the security guarantee for our protocol, we need a lower bound on  $H(\hat{A}_{\bar{x}}|E, \mathcal{V}_p)$  when the quantum probability distribution  $\{P(a, b|x, y)\}$  are observed.

We first introduce the converging upper bounds on the quantum relative entropy. For completeness, we follow the results in Ref. [27] and introduce the definitions here: a linear functional  $\rho$  on a von Neumann algebra  $\mathcal{A}$ ,  $\rho : \mathcal{A} \rightarrow \mathcal{C}$ , is said to be positive if  $\rho(a^*a) \geq 0$  for all  $a \in \mathcal{A}$ . A positive linear functional  $\rho$  is said to be a state if it satisfies  $\rho(I) = 1$ . The linear functional  $\rho$  can be defined by some trace-class operator  $\rho(a) = \text{Tr}[\tilde{\rho}a]$  for all  $a \in B(H)$ . To simplify notation, the same symbol  $\rho$  is used for both the positive linear functional  $\rho$  and the trace-class positive operator  $\tilde{\rho}$ . A sequence of converging variational upper bounds on the relative entropy is given by the following lemma:

**Lemma 1** (Brown, Fawzi, Fawzi, 2021 [27]). *let  $\rho, \sigma$  be two positive linear functionals on a von Neumann algebra  $\mathcal{A}$  such that  $\text{Tr}[\rho^2\sigma^{-1}] < \infty$ . Then for any  $m \in \mathbb{N}$  and the choice of  $t_1, \dots, t_m \in (0, 1]$  and  $w_1, \dots, w_m > 0$ , we have*

$$D(\rho||\sigma) \leq -\sum_{i=1}^m \frac{w_i}{t_i \ln 2} \inf_{a \in \mathcal{A}} \{\rho(I) + \rho(a + a^*) + (1 - t_i)\rho(a^*a) + \sigma(aa^*)\}. \quad (\text{A7})$$

Moreover, the right hand side converges to  $D(\rho||\sigma)$  as  $m \rightarrow \infty$ .

In the special case where  $\mathcal{A} = B(H)$  for a separable Hilbert space  $H$  and  $\rho$  and  $\sigma$  are defined via trace-class operators on  $H$ , satisfying  $\rho \leq \lambda\sigma$  for some  $\lambda \in \mathbb{R}_+$  (also denoted by  $\rho$  and  $\sigma$ ), we can give an explicit bound on the norm of the operators appearing in the optimization:

$$D(\rho||\sigma) \leq c_m - \sum_{i=1}^{m-1} \frac{w_i}{t_i \ln 2} \inf_{Z \in B(H), \|Z\| \leq \alpha_i} \{\text{Tr}[\rho(Z + Z^*)] + (1 - t_i)\text{Tr}[\rho Z^* Z] + t_i \text{Tr}[\sigma Z Z^*]\}, \quad (\text{A8})$$

where  $c_m = \frac{1}{m^2} \frac{\lambda \text{Tr}[\rho]}{\ln 2} - \sum_{i=1}^m \frac{w_i \text{Tr}[\rho]}{t_i \ln 2}$  and  $\alpha_i = \frac{3}{2} \max\{\frac{1}{t_i}, \frac{\lambda}{1-t_i}\}$ . Moreover, the right hand side converges to  $D(\rho||\sigma)$  as  $m \rightarrow \infty$ .

With Theorem. 1, now we can obtain a sequence of lower bounds on the conditional von Neumann entropy using the NPA hierarchy. Given a bipartite state  $\rho_{AB}$  on a joint Hilbert space  $H_A \otimes H_B$ , the conditional von Neumann entropy of  $A$  given  $B$  for the state  $\rho_{AB}$  is defined by the quantum relative entropy

$$H(A|B)_\rho := -D(\rho_{AB}||I_A \otimes \rho_B). \quad (\text{A9})$$

We consider positive trace-class operators here rather than the positive linear functionals on a von Neumann algebra  $\mathcal{A}$ . Hence, we say  $\rho$  is a state if  $\text{Tr}[\rho] = 1$ .

We shall now have the following Proposition to lower bound  $H(\hat{A}_{\bar{x}}|E, \mathcal{V}_p)$  by a converging sequence of optimizations that can be subsequently computed using the NPA hierarchy. The proof is based on the one used in [27], and we therefore explicitly extend the main result in [27] into the practical scenario with random post-selection and noisy pre-processing.

**Proposition 1.** *Let  $m \in \mathbb{N}$  and Let  $t_1, \dots, t_m$  and  $w_1, \dots, w_m$  be the nodes and weights of an  $m$ -point Gauss-Radau quadrature on  $[0, 1]$  with an endpoint  $t_m = 1$ . Let  $\rho_{ABE}$  be the initial quantum state shared between the devices of Alice, Bob and Eve and Let  $\{A_{a|\bar{x}}\}$  ( $\{B_{b|\bar{y}}\}$ ) denote the measurements operators performed by Alice's (Bob's) device in response to key-generation input  $X = \bar{x}$  ( $Y = \bar{y}$ ). let  $M_a = \frac{1}{p\mathcal{V}_p} \sum_{b=0}^1 \omega_{ab} A_{a|\bar{x}} \otimes B_{b|\bar{y}}$  and  $\hat{M}_a = (1-p_N) \cdot M_a + p_N \cdot M_{a+1}$  for  $a \in \{0, 1\}$ . Furthermore for  $i = 1, \dots, m-1$ , let  $\alpha_i = \frac{3}{2} \max\{\frac{1}{t_i}, \frac{1}{1-t_i}\}$ . Then  $H(\hat{A}_{\bar{x}}|E, \mathcal{V}_p)$  is never smaller than*

$$c_m + \sum_{i=1}^{m-1} \frac{w_i}{t_i \ln 2} \sum_a \inf_{Z_a \in B(Q_E)} \text{Tr} \left[ \rho_{ABE} \left( \hat{M}_a \otimes (Z_a + Z_a^* + (1 - t_i)Z_a^* Z_a) + t_i(\hat{M}_0 + \hat{M}_1) \otimes Z_a Z_a^* \right) \right] \quad (\text{A10})$$

$$\text{s.t. } \|Z_a\| \leq \alpha_i,$$

where  $c_m = -\frac{1}{m^2 \ln 2} + \sum_{i=1}^m \frac{w_i}{t_i \ln 2}$ . Moreover the lower bounds converge to  $H(\hat{A}_{\bar{x}}|E, \mathcal{V}_p)$  as  $m \rightarrow \infty$ .

*Proof.* Using Theorem. 1, let  $\rho_{\hat{A}E|\mathcal{V}_p} = \sum_a |a\rangle\langle a| \otimes \rho_{E|\mathcal{V}_p}(a, \bar{x})$  be the cq-state after Alice and Bob have performed the data preprocessing to the input  $(\bar{x}, \bar{y})$ , i.e.,  $\rho_{E|\mathcal{V}_p}(a, \bar{x}) = \text{Tr}_{Q_A Q_B}[\rho_{ABE}(\hat{M}_a \otimes I_E)]$ . Then for any  $m \in \mathbb{N}$  we have

$$\begin{aligned} H(\hat{A}_{\bar{x}}|E, \mathcal{V}_p) &= -D(\rho_{\hat{A}E|\mathcal{V}_p} || I_{\hat{A}|\mathcal{V}_p} \otimes \rho_{E|\mathcal{V}_p}) \quad (\text{A11}) \\ &\geq c_m + \sum_{i=1}^{m-1} \frac{w_i}{t_i \ln 2} \inf_{Z \in B(H)} \{ \text{Tr}[\rho_{\hat{A}E|\mathcal{V}_p}(Z + Z^*)] + (1 - t_i) \text{Tr}[\rho_{\hat{A}E|\mathcal{V}_p} Z^* Z] + t_i \text{Tr}[(I_{\hat{A}|\mathcal{V}_p} \otimes \rho_{E|\mathcal{V}_p}) Z Z^*] \} \\ \text{s.t. } & \|Z\| \leq \frac{3}{2} \max\left\{\frac{1}{t_i}, \frac{\lambda}{1 - t_i}\right\} \end{aligned}$$

with  $c_m = -\frac{\lambda}{m^2 \ln 2} + \sum_{i=1}^m \frac{w_i}{t_i \ln 2}$  and  $\lambda$  is some real number such  $\rho_{\hat{A}E|\mathcal{V}_p} \leq \lambda I_{\hat{A}|\mathcal{V}_p} \otimes \rho_{E|\mathcal{V}_p}$ . As system  $A$  is in a finite dimension, we can write the operator  $Z = \sum_{ab} |a\rangle\langle b| \otimes Z_{(a,b)}$  as some operators  $Z_{(a,b)} \in B(Q_E)$ . Then for the first term we have

$$\begin{aligned} \text{Tr}[\rho_{\hat{A}E|\mathcal{V}_p}(Z + Z^*)] &= \sum_a \text{Tr}[\rho_{E|\mathcal{V}_p}(a, \bar{x})(Z_{(a,a)} + Z_{(a,a)}^*)] \quad (\text{A12}) \\ &= \sum_a \text{Tr}[\text{Tr}_{Q_A Q_B}[\rho_{ABE}(\hat{M}_a \otimes I_E)](Z_{(a,a)} + Z_{(a,a)}^*)] \\ &= \sum_a \text{Tr}[\rho_{ABE}(\hat{M}_a \otimes (Z_{(a,a)} + Z_{(a,a)}^*))]. \end{aligned}$$

Repeating this for the second term, we have

$$\begin{aligned} \text{Tr}[\rho_{\hat{A}E|\mathcal{V}_p}(Z^* Z)] &= \sum_{ab} \text{Tr}[\rho_{E|\mathcal{V}_p}(a, \bar{x})(Z_{(a,b)}^* Z_{(a,b)})] \quad (\text{A13}) \\ &\geq \sum_a \text{Tr}[\rho_{E|\mathcal{V}_p}(a, \bar{x})(Z_{(a,a)}^* Z_{(a,a)})] \\ &= \sum_a \text{Tr}[\rho_{ABE}(\hat{M}_a \otimes Z_{(a,a)}^* Z_{(a,a)})]. \end{aligned}$$

where on the second line we have used the fact  $\sum_b Z_{(a,b)}^* Z_{(a,b)} \geq Z_{(a,a)}^* Z_{(a,a)}$ . Finally, for the third term

$$\begin{aligned} \text{Tr}[(I_{\hat{A}|\mathcal{V}_p} \otimes \rho_{E|\mathcal{V}_p}) Z Z^*] &= \sum_{ab} \text{Tr}[\rho_{E|\mathcal{V}_p} Z_{(a,b)} Z_{(a,b)}^*] \quad (\text{A14}) \\ &\geq \sum_a \text{Tr}[\rho_{E|\mathcal{V}_p} Z_{(a,a)}^* Z_{(a,a)}] \\ &= \sum_a \text{Tr}[\rho_{ABE}(\hat{M}_0 + \hat{M}_1) \otimes Z_{(a,a)}^* Z_{(a,a)}] \end{aligned}$$

As stated in the Ref. [27], one only need consider the operator  $Z$  that are block diagonal, i.e.,  $Z = \sum_a |a\rangle\langle a| \otimes Z_a$ . We hence recover the objective function stated in the proposition. Since  $\rho_{AE}$  is a cq-state we have  $\rho_{\hat{A}E|\mathcal{V}_p} \leq I_{\hat{A}|\mathcal{V}_p} \otimes \rho_{E|\mathcal{V}_p}$  and we can set  $\lambda = 1$ .  $\square$

The above proposition provide a converging sequence of lower bounds on the conditional von Neumann entropy. Using the NPA hierarchy [49, 56], we can turn these lower bounds into a device-independent situation. The lower bounds on the rate of a device-independent protocol can be obtained by including the optimizations of all states, measurements and Hilbert spaces, subjecting to any constraints on the devices' joint probability distribution  $\{P(a, b|x, y)\}$  which involves all outcomes without post-selection to ensure that there are no detection loopholes. Following [27], a lower bound which converges fastly on  $H(\hat{A}_{\bar{x}}|E, \mathcal{V}_p)$  for all possible devices can be solved by a sequence of SDPs

optimization problem:

$$\begin{aligned}
c_m + \sum_{i=1}^{m-1} \frac{w_i}{t_i \ln 2} \inf \sum_{a=0}^1 & \left[ \langle \psi | \hat{M}_a (Z_{a,i} + Z_{a,i}^* + (1-t_i) Z_{a,i}^* Z_{a,i}) + t_i (\hat{M}_0 + \hat{M}_1) Z_{a,i} Z_{a,i}^* | \psi \rangle \right] & (A15) \\
\text{s.t. } & \langle \psi | A_{a|x} B_{b|y} | \psi \rangle = P(ab|xy), \quad \text{for all } a, b, x, y \\
& \sum_a A_{a|x} = \sum_b B_{b|y} = I, \quad \text{for all } x, y \\
& A_{a|x} \geq 0, \quad B_{b|y} \geq 0 \quad \text{for all } a, b, x, y \\
& Z_{a,i} Z_{a,i}^* \leq \alpha_i \quad \text{for all } a, i \\
& Z_{a,i}^* Z_{a,i} \leq \alpha_i \quad \text{for all } a, i \\
& [A_{a|x}, B_{b|y}] = [A_{a|x}, Z_{a,i}^{(*)}] = [B_{a|x}, Z_{a,i}^{(*)}] \quad \text{for all } a, b, x, y, i \\
& A_{a|x}, B_{b|y}, Z_{a,i} \in B(H) \quad \text{for all } a, b, x, y, i
\end{aligned}$$

where we have considered the pure states and dropped the tensor product structure [27].

### 3. Simulations

For a demonstration of DI-QKD with photonic devices, we derive a model to consider experimental imperfections and perform numerical simulations to optimize the implementation parameters. Our model includes the imperfections in the measurement devices such as dark counts, and in the entanglement source such as the non-ideal fidelity, multiple photon pairs and so forth. These imperfections turns out to be the main cause of additional unwanted noise and the very low Bell violation, which makes it quite difficult to demonstrate a photonic DI-QKD [57].

We first construct the model here. In the experiment, the SPDC source is employed to produce a bipartite state while polarization beamsplitters and non-photon number resolving detectors are employed to perfrom measurements. In front of the detector, a set of wave-plates is used to choose the local measurement setting. In such an optical implementation, each of the measurements applied by Alice and Bob has two possible outcomes: click or no-click on the detector. In our simulation, we label that a click on the detector as “0” and no-click as “1”.

For the imperfections of the input state, the most general way is to use the visibility to quantify the prepared state. Here, we model the prepared state by

$$\rho = V \times \frac{1}{1+r^2} \begin{pmatrix} 0 & 0 & 0 & 0 \\ 0 & 1 & r & 0 \\ 0 & r & r^2 & 0 \\ 0 & 0 & 0 & 0 \end{pmatrix} + (1-V) \times \frac{I}{4}, \quad (A16)$$

where  $V$  denotes the visibility along a certain measurement direction, and we suppose the visibility to be 0.992 in experiments.

For simplicity, we restrict to projective measurements within the  $x$ - $z$  plane of the Bloch-sphere, i.e., measurements  $\{\Pi(\phi), 1 - \Pi(\phi)\}$ , with the projectors defined by  $\Pi(\phi) = \begin{pmatrix} \cos^2(\phi/2) & \cos(\phi/2) \sin(\phi/2) \\ \cos(\phi/2) \sin(\phi/2) & \sin^2(\phi/2) \end{pmatrix}$ , for  $\phi \in [0, \pi/2]$ . Since each party effectively produces one of two possible outcomes, 0 or 1, the devices’ behaviour for a single pair of photons can be written as  $p(a, b|x, y) = \text{Tr}[\rho(A_{a|x} \otimes B_{b|y})]$ , where  $A_{a|x}$  and  $B_{b|y}$  are defined as

$$\begin{aligned}
A_{0|x} &= (1 - (1 - p_d)(1 - \eta)) \frac{I + \Pi(\phi_x)}{2} + p_d \cdot \frac{I - \Pi(\phi_x)}{2}, \quad A_{1|x} = I - A_{0|x}, \\
B_{0|y} &= (1 - (1 - p_d)(1 - \eta)) \frac{I + \Pi(\phi_y)}{2} + p_d \cdot \frac{I - \Pi(\phi_y)}{2}, \quad B_{1|x} = I - B_{0|x},
\end{aligned} \quad (A17)$$

Here,  $\eta \in [0, 1]$  is the detection efficiency of the inefficient detectors.  $p_d = 10^{-6}$  is the dark count probability of a single detector.

In the experiment, we have to also consider that the photon source may emit multiple pairs of photons. The photon pair distribution of a SPDC source follows a Poisson type, i.e.

$$P(n) = e^{-\mu} \frac{\mu^n}{n!}. \quad (A18)$$

That is, the source may emit vacuum with probability  $P(0)$ , one pair with probability  $P(1)$ , two pairs with probability  $P(2)$ , and so on. As the probability of multiple photon pairs is very small, we only consider three photon pairs as input. For each photon pair, there are four possible and also exclusive events  $\{00, 01, 10, 11\}$ . Suppose that the underlying probability distribution of the four events with single photon pair conditioned on specific input setting  $(x, y)$  are denoted by  $p_k(x, y)$ , where  $k$  is the  $k_{th}$  event. Then we can calculate the probabilities with two pairs of photons after the assignment by

$$p_k^{\text{2-pairs}}(x, y) = \sum_{i,j} \beta_{i,j}^{(k)} p_i(x, y) p_j(x, y), \text{ for } k=1,2,3,4. \quad (\text{A19})$$

We here give the four coefficients  $\beta_{i,j}^k$ ,

$$\beta_{i,j}^{(1)} = \begin{pmatrix} 1 & 1 & 1 & 1 \\ 1 & 0 & 1 & 0 \\ 1 & 1 & 0 & 0 \\ 1 & 0 & 0 & 0 \end{pmatrix}, \beta_{i,j}^{(2)} = \begin{pmatrix} 0 & 0 & 0 & 0 \\ 0 & 1 & 0 & 1 \\ 0 & 0 & 0 & 0 \\ 0 & 1 & 0 & 0 \end{pmatrix}, \beta_{i,j}^{(3)} = \begin{pmatrix} 0 & 0 & 0 & 0 \\ 0 & 0 & 0 & 0 \\ 0 & 0 & 1 & 1 \\ 0 & 0 & 1 & 0 \end{pmatrix}, \beta_{i,j}^{(4)} = \begin{pmatrix} 0 & 0 & 0 & 0 \\ 0 & 0 & 0 & 0 \\ 0 & 0 & 0 & 0 \\ 0 & 0 & 0 & 1 \end{pmatrix}. \quad (\text{A20})$$

The probabilities with three pairs of photons can be calculated by

$$p_k^{\text{3-pairs}}(x, y) = \sum_{i,j} \beta_{i,j}^k p_i^{\text{2-pairs}}(x, y) p_j(x, y). \quad (\text{A21})$$

Combined these results, the joint conditional distribution  $P(a, b|x, y)$  can be calculated as

$$\begin{aligned} P(0, 0|x, y) &= \exp(-u) \sum_{n=0}^3 \frac{u^n}{n!} \cdot p_1^{\text{n-pairs}}(x, y), \\ P(0, 1|x, y) &= \exp(-u) \sum_{n=0}^3 \frac{u^n}{n!} \cdot p_2^{\text{n-pairs}}(x, y), \\ P(10|x, y) &= \exp(-u) \sum_{n=0}^3 \frac{u^n}{n!} \cdot p_3^{\text{n-pairs}}(x, y), \\ P(1, 1|x, y) &= \exp(-u) \sum_{n=0}^3 \frac{u^n}{n!} \cdot p_4^{\text{n-pairs}}(x, y). \end{aligned} \quad (\text{A22})$$

It should be noted that, since the dark count is independent of the input measurement settings, the probabilities  $p_k^{\text{0-pairs}}(x, y)$  with no photons are  $\{p_d^2, p_d(1 - p_d), p_d(1 - p_d), (1 - p_d)^2\}$ .

With this model, we construct a numerical tool to compute the secret key rate [27] and optimize the experiment parameters. Our main result is shown as the purple-solid curve in Fig. 4. We compute the key rate with the Gauss-Radau quadrature of  $m = 8$  nodes and the results are calculated at a relaxation level  $2+ABZ+AZZ$ . We first consider the protocol without any data preprocesses. If the experimental imperfections are ignored, i.e., with ideal devices, the results are shown as the red-dashed curve in Fig. 4 where a positive key can be achieved if the global detection efficiency is around 83% [27]. When taking the imperfections into account, as the blue dotted-dashed curve in Fig. 4 shows, a minimum global detection efficiency of  $\eta \approx 91.2\%$  is needed to have a positive key rate. Nevertheless, after considering the date preprocesses of post-selection and noisy preprocessing, by optimizing the probabilities  $(p, p_N)$  at each data point, a positive key rate can only be reached with a minimal required efficiency of 86.2%. This value is out of reach for all previous photonic experiments on Bell test and related applications [12–24].

## Appendix B: Analysis method

### 1. Conditional probabilities Processing

In our experiments, the quantum conditional von Neumann entropy  $H(\hat{A}_{\bar{x}}|E, \mathcal{V}_p)$  is bounded by the complete set of probabilities  $\{P(a, b|x, y)\}$ . We first introduce the set of quantum distributions  $\mathcal{Q}$ , i.e., the set of behaviors such that there exist a 2-partite quantum state  $\rho$  shared by Alice and Bob and local measurements  $A_{a|x}$  and  $B_{b|y}$  yielding the outcomes  $(a, b)$  a with probability  $P(a, b|x, y)$  when performing the measurements  $(x, y)$ . Follows from Born's rule,

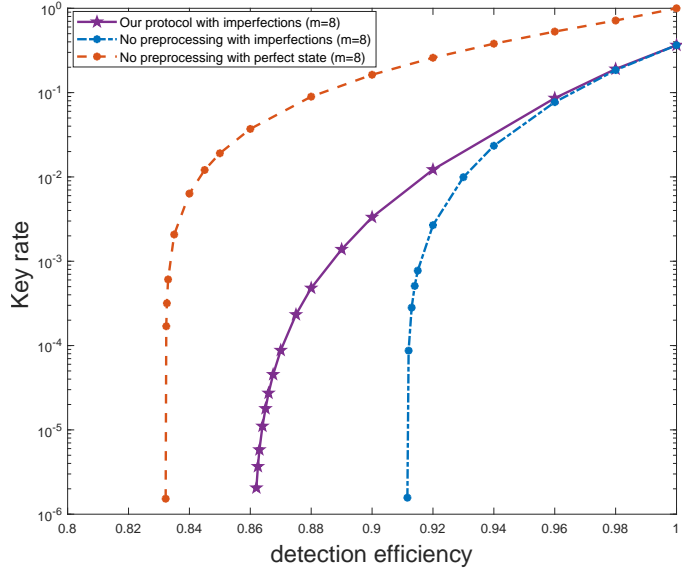


FIG. 4. Secret key rate as a function of detection efficiency. By incorporating post-selection and noisy preprocessing, our protocol can tolerate efficiency as low as  $\eta \approx 86.2\%$  (purple-solid curve). The blue dot-dashed curve is protocol without any preprocessing, which shows positive key rate with threshold efficiency  $\eta \approx 91.2\%$ . If one considers ideal devices, the protocol without any preprocessing can achieve a positive key rate at  $\eta \approx 83\%$ .

the conditional probability distributions read as  $P(a, b|x, y) = \text{Tr}(\rho A_{a|x} \otimes B_{b|y})$ . Importantly, quantum distributions satisfy the no-signaling conditions, i.e., their marginal distributions are independent of the measurement choice of the distant party.

In experiment, the observed distribution  $P(a, b|x, y)$  is estimated by computing the relative frequency, i.e.,  $f(a, b|x, y) = \frac{N_{a,b,x,y}}{N_{x,y}}$  where  $N_{a,b,x,y}$  is the number of detection events  $(a, b, x, y)$  registered and  $N_{x,y} = \sum_{a,b} N_{a,b,x,y}$  is the total number of trials corresponding to the measurement choice  $(x, y)$ . However, due to the the statistical fluctuations, the original relative frequency  $f(a, b|x, y)$  may not meet the no-signaling constrain. Hence, the estimated behavior  $P(a, b|x, y)$  cannot be used directly to compute the key rate.

For this, we determine an conditional distribution  $P(a, b|x, y)$  by the least-square problem [58] using the calibration data to ensure that  $P(a, b|x, y)$  follows from the rule of quantum distributions.

$$\begin{aligned} & \min \|\vec{P} - \vec{f}\|_2 \\ & \text{s.t. } P(a, b|x, y) \in \mathcal{Q}, \end{aligned} \tag{B1}$$

where we refer to the complete set of quantum distribution  $\{P(a, b|x, y)\}$  as a vector  $\vec{P}$  and  $\|\cdot\|_p$  denotes the  $p$ -norm.

## 2. Dual solution and Confidence region

The dual solution of 1 provides us with an affine function

$$g(\vec{P}) = \alpha + \sum_{a,b,x,y} \lambda_{a,b,x,y} P(a, b|x, y), \tag{B2}$$

which is always an upper bound on the primal program 1. As already observed in [54],  $g(\vec{P})$  can be seen as the “optimal” Bell expressions, i.e., the amount of  $H(\hat{A}_{\bar{x}}|E, \mathcal{V}_p)$  certified from the Bell expressions  $g(\vec{P})$  is equal to the amount of  $H(\hat{A}_{\bar{x}}|E, \mathcal{V}_p)$  that can be certified from the full set of probabilities  $\{P(a, b|x, y)\}$ .

Note that there are 24 different probabilities  $P(a, b|x, y)$  and thus 24 associated Bell expressions  $e_1, \dots, e_{24}$  defined by  $e_t(\hat{P}) = P(a, b|x, y)$ , with one value of  $t$  for each of the possible event of  $(a, b, x, y)$ . But since the probabilities satisfy normalization and no-signaling, they can be uniquely specified by the 11 probabilities, which constitute 11 Bell expressions  $h_1, \dots, h_{11}$ , where  $h_1$  and  $h_2$  are the Alice’s two marginal probabilities  $P_A(1|x)$ ,  $h_3, h_4$  and  $h_5$  are the

Bob's three marginal probabilities  $P_B(1|y)$ , and  $h_6, \dots, h_{11}$  are the six bipartite correlators  $P(1, 1|x, y)$ . In this sense, the dual solution B2 could be represented by

$$g(\vec{P}) = \beta + \sum_t \gamma_t h_t, \quad (\text{B3})$$

where  $\alpha$  is a real constant. Looking at the dual solution of the simulation at  $\eta = 0.875$ , we can extract the function

$$\begin{aligned} g(\hat{P}) = & -1.2951 + 0.8564P(1, 1|1, 1) + 0.8437P(1, 1|1, 2) - 0.05783P(1, 1|1, 3) + 0.8565P(1, 1|2, 1) \\ & - 1.1736P(1, 1|2, 2) + 0.003611P(1, 1|2, 3) + 0.09415P_A(1|1) + 0.3155P_A(1|2) \\ & - 0.8432P_B(1|1) + 0.3312P_B(1|2) + 0.9027P_B(1|3), \end{aligned} \quad (\text{B4})$$

which lower bounds  $H(\hat{A}_{\bar{x}}|E, \mathcal{V}_p)$ .

Using the the straightforward estimator for the Bell expectations  $g(\vec{P})$ , we can construct a confidence region for our  $n$ -round experiments. Let  $\mathcal{X}(a, b, x, y)$  be the indicator function for the event  $\{a, b, x, y\}$ , i.e.,  $\mathcal{X} = 1$  if the event  $\{a, b, x, y\}$  is observed and  $\mathcal{X} = 0$  otherwise. Consider the following random variable for the  $i_{\text{th}}$ -round

$$g'_i = g_i - \alpha = \sum_{a, b, x, y} \lambda_{a, b, x, y} \frac{\mathcal{X}(a = a_i, b = b_i, x = x_i, y = y_i)}{P(x_i, y_i)}, \quad (\text{B5})$$

since we have assumed that the devices are memoryless and behave identically and independently at each step of the protocol, we thus could have the expected value  $E[g'_i] = g(\vec{P}) - \alpha$  and  $|g_i| \leq \lambda/q$ , where  $\lambda = \max |\lambda_{a, b, x, y}|$  and  $q = \max P(x, y)$ . Defining the resulting estimators  $\hat{g}'$  for the Bell expectations  $g(\vec{P}) - \alpha$  by the observed frequencies  $\hat{g}'_i$ ,

$$\hat{g}' = \frac{1}{n} \sum_{i=1}^n \hat{g}'_i = \frac{1}{n} \sum_{i=1}^n \frac{\lambda_{a_i, b_i, x_i, y_i}}{P(x_i, y_i)}. \quad (\text{B6})$$

As a consequence of the Hoeffding's inequality, we have

$$\Pr[|g(\vec{P}) - (\hat{g}' + \alpha)| \geq \delta] \leq 2\epsilon. \quad (\text{B7})$$

where  $\epsilon = \exp\left(\frac{-2n\delta^2}{(2\lambda/q)^2}\right)$ .

## Appendix C: System characterization

### 1. Determination of single photon efficiency

We focus the pump and collection mode to the center of the PPKTP crystal [59]. In experiment, the light is focused using an aspherical lens with  $f = 8 \text{ mm}$  to the PPKTP that is around  $70 \text{ cm}$  away. The pump waist is estimated to be  $200 \mu\text{m}$ . An aspherical lens with  $f = 9.6 \text{ mm}$  and two spherical lenses with  $f = 150 \text{ mm}$  and  $f = -150 \text{ mm}$  focus the beam to  $97.5 \mu\text{m}$  at the center of PPKTP. The spherical lenses are placed in the middle. The distance between them is about  $12.5 \text{ cm}$ , about  $70 \text{ cm}$  from the aspherical lens and about  $33.5 \text{ cm}$  from the PPKTP.

We define the single photon heralding efficiency as  $\eta_A = C/N_B$  and  $\eta_B = C/N_A$  for Alice and Bob, in which two-photon coincidence events  $C$  and single photon detection events for Alice  $N_A$  and Bob  $N_B$  are measured in the experiment. The heralding efficiency is listed in Tab. IV, where  $\eta^{\text{sc}}$  is the efficiency of coupling entangled photons into single mode optical fiber,  $\eta^{\text{so}}$  the optical efficiency due to limited transmittance of optical elements in the source, and  $\eta^{\text{det}}$  the single photon detector efficiency.  $\eta^{\text{so}}$ ,  $\eta^{\text{det}}$  can be measured with classical light beams and NIST-traceable power meters. The optical transmittance for all involved optical elements are listed in Tab. V, with which we obtain the optical efficiency  $\eta^{\text{so}}$ :

$$\begin{cases} \eta^{\text{so}}(\text{Alice}) = \eta^{\text{AS}} \times (\eta^{\text{S}})^2 \times (\eta^{\text{DM}})^7 \times \eta^{780/1560\text{HWP}} \times \eta^{780/1560\text{PBS}} \times \eta^{\text{PPKTP}} \times \eta^{1560\text{HWP}} \times \eta^{1560\text{QWP}} \times \eta^{1560\text{PBS}} \\ \eta^{\text{so}}(\text{Bob}) = \eta^{\text{AS}} \times (\eta^{\text{S}})^2 \times (\eta^{\text{DM}})^8 \times \eta^{780/1560\text{HWP}} \times \eta^{780/1560\text{PBS}} \times \eta^{\text{PPKTP}} \times \eta^{1560\text{HWP}} \times \eta^{1560\text{QWP}} \times \eta^{1560\text{PBS}} \end{cases} \quad (\text{C1})$$

TABLE IV. Characterization of optical efficiencies in the experiments.

	heralding efficiency ( $\eta$ )	$\eta^{\text{sc}}$	$\eta^{\text{so}}$	$\eta^{\text{det}}$
Alice	87.16%	95.57%	93.53%	97.51%
Bob	87.82%	95.74%	93.03%	98.60%

TABLE V. The efficiencies of optical elements.

Optical element	Efficiency
Aspherical lens	$99.27\% \pm 0.03\%$
Spherical lens	$99.6\% \pm 1.0\%$
Half wave plate (780nm/1560nm)	$99.93\% \pm 0.02\%$
Half wave plate (1560nm)	$99.92\% \pm 0.04\%$
Quarter wave plate (1560nm)	$99.99\% \pm 0.08\%$
Polarizing beam splitter (780nm/1560nm)	$99.6\% \pm 0.1\%$
Polarizing beam splitter (1560nm)	$99.6\% \pm 0.2\%$
Dichoric mirror	$99.46\% \pm 0.03\%$
PPKTP	$99.6\% \pm 0.2\%$

## 2. Quantum state and measurement bases

To optimize the generated key rate for our experiment, we aim to create a non-maximally entangled two-photon state  $\cos(\alpha)|HV\rangle + \sin(\alpha)|VH\rangle$ , where  $\alpha = 20.0^\circ$  and set measurement bases to be  $x_1 = -88.22^\circ$  and  $x_2 = 54.29^\circ$  for Alice, and  $y_1 = 9.75^\circ$ ,  $y_2 = 21.45^\circ$  and  $y_3 = -1.07^\circ$  for Bob, respectively. We also optimize the mean photon number to be 0.04 to maximize the key rate.

We perform quantum state tomography measurement of the non-maximally entangled state, with result shown in Fig. 5. The state fidelity is  $99.52 \pm 0.15\%$ . We attribute the imperfection to multi-photon components, imperfect optical elements, and imperfect spatial/spectral mode matching.

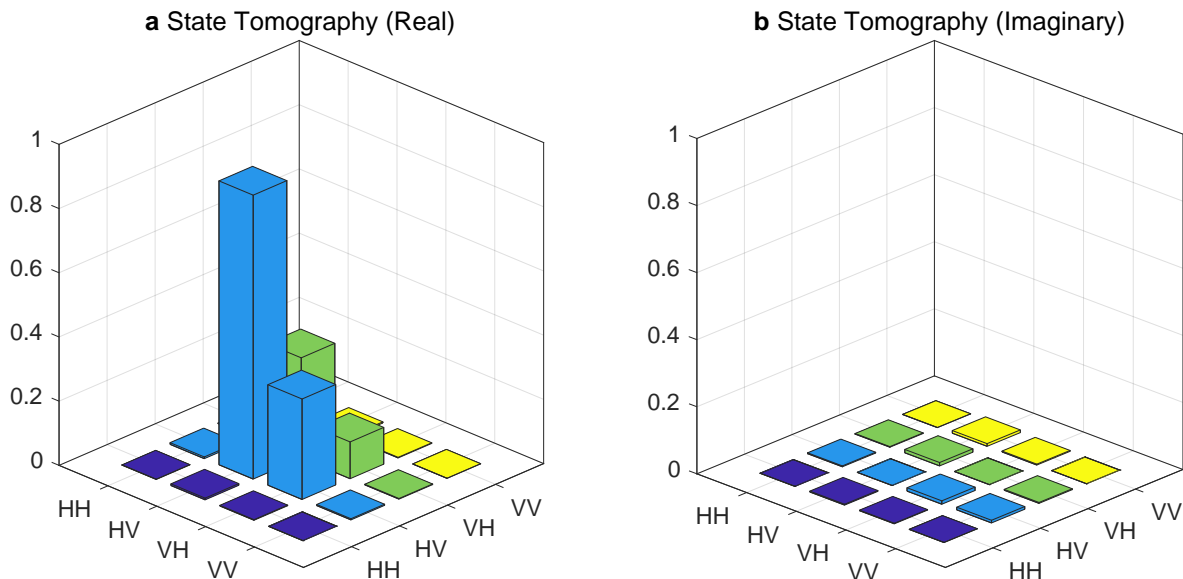


FIG. 5. (color online) Tomography of the produced two-photon state in the experiments, with real and imaginary components shown in a and b.

## Appendix D: Experimental results

### 1. CHSH test

Before the start of the experiment, systematic experimental calibrations are implemented to optimize a CHSH [60]Bell test based on the performance of system. We optimize to create a non-maximally entangled two-photon state  $\cos(\alpha)|HV\rangle + \sin(\alpha)|VH\rangle$ , where  $\alpha = 32.2^\circ$  and set measurement bases to be  $x_1 = -81.09^\circ$  and  $x_2 = 61.46^\circ$  for Alice, and  $y_1 = 8.18^\circ$  and  $y_2 = -29.37^\circ$  for Bob, respectively. We also optimize the mean photon number to be 0.62 to maximize the CHSH score. The CHSH score  $\omega_{\text{CHSH}}$  is given by

$$\omega_{\text{CHSH}} = \sum_{k,l} \sum_{i=1}^{n_{x_i y_i = kl}} (1 + (-1)^{a_i \oplus b_i \oplus (x_i \cdot y_i)}) / n_{x_i y_i = kl}, \quad (\text{D1})$$

with  $(k, l) \in (0, 1) \times (0, 1)$  is computed to be 0.7559. The recorded data are shown in Fig. 6.

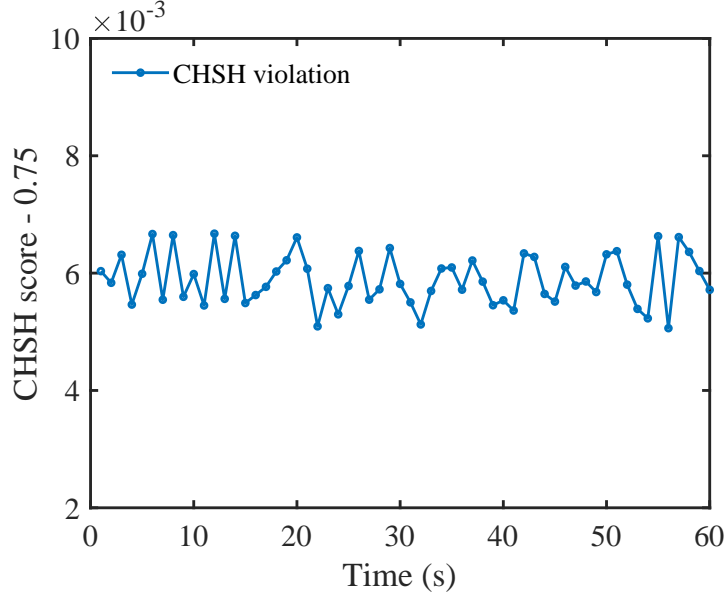


FIG. 6. **CHSH violation versus time.** We conduct  $1.2 \times 10^7$  rounds of CHSH tests at a repetition rate of 200 KHz. We choose the average value of CHSH violations for each 1 second data as a point to observe its performance.

### 2. Experimental data analysis

The implementation of the protocol depends on numerical studies shown in section A 3. We conduct  $2.4 \times 10^8$  rounds of experiment for each of the six combinations of measurement settings  $(x, y)$  at a repetition rate of  $2 \times 10^6$ . The counts are shown in Tab. VI. According to the method described in section B 1, we first optimize the probability distribution  $P(a, b|x, y)$  under the no-signaling condition [61] and Tsirelson's bounds [62]. The results are shown in Tab. VII. Based on the method described in section B 2, we set the error probability  $\epsilon = 10^{-2}$ . For the experiment of 20 m fiber length,  $\lambda \approx 3.15$  is calculated according to  $P(a, b|x, y)$ . Thus we could have  $\delta \approx 0.0015$  representing the confidence region of  $H(\hat{A}_x|E, \mathcal{V}_p)$ . While for the experiment of 80 m fiber length,  $\lambda \approx 2.36$ , and  $\delta \approx 0.0011$ . In the experiment of 220 m fiber length,  $\lambda \approx 6.66 \times 10^{-2}$ , and  $\delta \approx 3.20 \times 10^{-5}$ . It should be noted that  $\delta$  is proportional to  $1/\sqrt{n}$ , indicating a lower bound with more experimental rounds.

[1] C. H. Bennett and G. Brassard, in *Proceedings of IEEE International Conference on Computers, Systems and Signal Processing* (Bangalore, India, 1984) pp. 175–179.

TABLE VI. **Counts of experimental rounds.** Recorded number of two-photon detection events for six sets of polarization state measurement bases  $x = 1$  or  $2$  indicates two different settings and  $y = 1, 2$  or  $3$  indicates three different settings.  $a(b) = 0$  or  $1$  indicates that Alice(Bob) detects a photon or not.

Fiber length/m	Basis settings	$ab = 11$	$ab = 10$	$ab = 01$	$ab = 00$
20	$xy = 11$	238565091	403056	210284	821569
	$xy = 12$	237797832	1164958	225388	811822
	$xy = 13$	238783108	162648	160633	893611
	$xy = 21$	236368886	222941	2390061	1018112
	$xy = 22$	234578742	1973697	3385904	61657
	$xy = 23$	236058614	516659	2882175	542552
80	$xy = 11$	238758474	350531	182413	708582
	$xy = 12$	238128577	998486	190177	682760
	$xy = 13$	238971836	142160	136010	749994
	$xy = 21$	236913121	197393	2020739	868747
	$xy = 22$	235413651	1674701	2863370	48278
	$xy = 23$	236655191	441918	2442392	460499
220	$xy = 11$	238531173	422523	221542	824762
	$xy = 12$	237751528	1191525	236435	820512
	$xy = 13$	238808826	168059	164710	858405
	$xy = 21$	236390264	231282	2373297	1005157
	$xy = 22$	234718386	1924194	3299222	58198
	$xy = 23$	236077278	517035	2869523	536164

TABLE VII. The input-output probability distribution  $p(a, b|x, y)$ . A 2-norm estimation is applied to the data to derive a probability distribution adapted to the model used.

Fiber length/m	$(x, y)$	$(a, b)$			
		11	10	01	00
20	11	0.9939848305625	0.0016772430375	0.0008783402625	0.0034595861375
	12	0.9907551763625	0.0049068972375	0.0008862111125	0.0034517152875
	13	0.9949539201500	0.0007081534400	0.0006388507000	0.0036990757000
	21	0.9848486222042	0.0008729597292	0.0100145486208	0.0042638694458
	22	0.9775156493042	0.0082059326292	0.0141257381708	0.0001526798958
	23	0.9835762722167	0.0021453097167	0.0120164986333	0.0022619194333
80	11	0.9948356614583	0.0014838718733	0.0007367281267	0.0029437385417
	12	0.9921373177096	0.0041822156221	0.0007705468779	0.0029099197904
	13	0.9957109010408	0.0006086322908	0.0005504093742	0.0031300572942
	21	0.9871206246575	0.0007904517325	0.0084517649275	0.0036371586825
	22	0.9809551559062	0.0069559204838	0.0119527086813	0.0001362149287
	23	0.9860772142350	0.0018338621550	0.0101840961800	0.0019048274300
220	11	0.9938998979150	0.0017579270850	0.0009256770850	0.0034164979150
	12	0.9906931322925	0.0049646927075	0.0009851406225	0.0033570343775
	13	0.9949693281250	0.0006884968750	0.0006980406250	0.0036441343750
	21	0.9849438305550	0.0009706680550	0.0098817444450	0.0042037569450
	22	0.9779142690975	0.0080002295125	0.0137640038175	0.0003214975725
	23	0.9837356045150	0.0021788940950	0.0119317642350	0.0021537371550

- [2] A. K. Ekert, *Phys. Rev. Lett.* **67**, 661 (1991).
- [3] F. Xu, X. Ma, Q. Zhang, H.-K. Lo, and J.-W. Pan, *Reviews of Modern Physics* **92**, 025002 (2020).
- [4] D. Mayers and A. Yao, in *Proceedings of the 39th Annual Symposium on Foundations of Computer Science*, FOCS '98 (IEEE Computer Society, Washington, DC, USA, 1998) pp. 503–.
- [5] J. Barrett, L. Hardy, and A. Kent, *Phys. Rev. Lett.* **95**, 010503 (2005).
- [6] A. Acín, N. Brunner, N. Gisin, S. Massar, S. Pironio, and V. Scarani, *Phys. Rev. Lett.* **98**, 230501 (2007).
- [7] S. Pironio, A. Acín, N. Brunner, N. Gisin, S. Massar, and V. Scarani, *New. J. Phys.* **11**, 045021 (2009).
- [8] L. Masanes, S. Pironio, and A. Acín, *Nat. Commn.* **2**, 238 (2011).
- [9] B. W. Reichardt, F. Unger, and U. Vazirani, *Nature* **496**, 456 (2013).
- [10] U. Vazirani and T. Vidick, *Phys. Rev. Lett.* **113**, 140501 (2014).
- [11] R. Arnon-Friedman, F. Dupuis, O. Fawzi, R. Renner, and T. Vidick, *Nat. Commn.* **9**, 459 (2018).
- [12] M. Giustina, A. Mech, S. Ramelow, B. Wittmann, J. Kofler, J. Beyer, A. Lita, B. Calkins, T. Gerrits, S. W. Nam, *et al.*, *Nature* **497**, 227 (2013).

[13] B. G. Christensen, K. T. McCusker, J. B. Altepeter, B. Calkins, T. Gerrits, A. E. Lita, A. Miller, L. K. Shalm, Y. Zhang, S. W. Nam, *et al.*, *Physical review letters* **111**, 130406 (2013).

[14] L. K. Shalm, E. Meyer-Scott, B. G. Christensen, P. Bierhorst, M. A. Wayne, M. J. Stevens, T. Gerrits, S. Glancy, D. R. Hamel, M. S. Allman, K. J. Coakley, S. D. Dyer, C. Hodge, A. E. Lita, V. B. Verma, C. Lambrocco, E. Tortorici, A. L. Miggall, Y. Zhang, D. R. Kumor, W. H. Farr, F. Marsili, M. D. Shaw, J. A. Stern, C. Abellán, W. Amaya, V. Pruneri, T. Jennewein, M. W. Mitchell, P. G. Kwiat, J. C. Bienfang, R. P. Mirin, E. Knill, and S. W. Nam, *Phys. Rev. Lett.* **115**, 250402 (2015).

[15] M. Giustina, M. A. M. Versteegh, S. Wengerowsky, J. Handsteiner, A. Hochrainer, K. Phelan, F. Steinlechner, J. Kofler, J.-A. Larsson, C. Abellán, W. Amaya, V. Pruneri, M. W. Mitchell, J. Beyer, T. Gerrits, A. E. Lita, L. K. Shalm, S. W. Nam, T. Scheidl, R. Ursin, B. Wittmann, and A. Zeilinger, *Phys. Rev. Lett.* **115**, 250401 (2015).

[16] M.-H. Li, C. Wu, Y. Zhang, W.-Z. Liu, B. Bai, Y. Liu, W. Zhang, Q. Zhao, H. Li, Z. Wang, *et al.*, *Physical review letters* **121**, 080404 (2018).

[17] Y. Liu, X. Yuan, M.-H. Li, W. Zhang, Q. Zhao, J. Zhong, Y. Cao, Y.-H. Li, L.-K. Chen, H. Li, *et al.*, *Physical review letters* **120**, 010503 (2018).

[18] L. Shen, J. Lee, J.-D. Bancal, A. Cerè, A. Lamas-Linares, A. Lita, T. Gerrits, S. W. Nam, V. Scarani, C. Kurtsiefer, *et al.*, *Physical review letters* **121**, 150402 (2018).

[19] P. Bierhorst, E. Knill, S. Glancy, Y. Zhang, A. Mink, S. Jordan, A. Rommal, Y.-K. Liu, B. Christensen, S. W. Nam, *et al.*, *Nature* **556**, 223 (2018).

[20] Y. Liu, Q. Zhao, M.-H. Li, J.-Y. Guan, Y. Zhang, B. Bai, W. Zhang, W.-Z. Liu, C. Wu, X. Yuan, *et al.*, *Nature* **562**, 548 (2018).

[21] Y. Zhang, L. K. Shalm, J. C. Bienfang, M. J. Stevens, M. D. Mazurek, S. W. Nam, C. Abellán, W. Amaya, M. W. Mitchell, H. Fu, *et al.*, *Physical Review Letters* **124**, 010505 (2020).

[22] W.-Z. Liu, M.-H. Li, S. Ragy, S.-R. Zhao, B. Bai, Y. Liu, P. J. Brown, J. Zhang, R. Colbeck, J. Fan, *et al.*, *Nature Physics* **17**, 448 (2021).

[23] M.-H. Li, X. Zhang, W.-Z. Liu, S.-R. Zhao, B. Bai, Y. Liu, Q. Zhao, Y. Peng, J. Zhang, Y. Zhang, W. J. Munro, X. Ma, Q. Zhang, J. Fan, and J.-W. Pan, *Phys. Rev. Lett.* **126**, 050503 (2021).

[24] L. K. Shalm, Y. Zhang, J. C. Bienfang, C. Schlager, M. J. Stevens, M. D. Mazurek, C. Abellán, W. Amaya, M. W. Mitchell, M. A. Alhejji, *et al.*, *Nature Physics* **17**, 452 (2021).

[25] F. Xu, Y.-Z. Zhang, Q. Zhang, and J.-W. Pan, [arXiv:2110.02701](https://arxiv.org/abs/2110.02701) (2021).

[26] M. Ho, P. Sekatski, E.-Z. Tan, R. Renner, J.-D. Bancal, and N. Sangouard, *Physical Review Letters* **124**, 230502 (2020).

[27] P. Brown, H. Fawzi, and O. Fawzi, (2021), [arXiv:2106.13692](https://arxiv.org/abs/2106.13692).

[28] H. K. Lo and H. F. Chau, *Science* **283**, 2050 (1999).

[29] P. W. Shor and J. Preskill, *Phys. Rev. Lett.* **85**, 441 (2000).

[30] R. Renner, *Int. J. Quantum Inf.* **06**, 1 (2008).

[31] F. Xu, B. Qi, and H.-K. Lo, *New. J. Phys.* **12**, 113026 (2010).

[32] L. Lydersen, C. Wiechers, C. Wittmann, D. Elser, J. Skaar, and V. Makarov, *Nat. Photon.* **4**, 686 (2010).

[33] H.-K. Lo, M. Curty, and B. Qi, *Phys. Rev. Lett.* **108**, 130503 (2012).

[34] S. L. Braunstein and S. Pirandola, *Phys. Rev. Lett.* **108**, 130502 (2012).

[35] M. Lucamarini, Z. Yuan, J. Dynes, and A. Shields, *Nature* **557**, 400 (2018).

[36] J. Barrett, R. Colbeck, and A. Kent, *Phys. Rev. Lett.* **110**, 010503 (2013).

[37] M. Curty and H.-K. Lo, *Npj Quantum Inf.* **5**, 14 (2019).

[38] B. Hensen, H. Bernien, A. E. Dréau, A. Reiserer, N. Kalb, M. S. Blok, J. Ruitenberg, R. F. L. Vermeulen, R. N. Schouten, C. Abellán, W. Amaya, V. Pruneri, M. W. Mitchell, M. Markham, D. J. Twitchen, D. Elkouss, S. Wehner, T. H. Taminiau, and R. Hanson, *Nature* **526**, 682 (2015).

[39] W. Rosenfeld, D. Burchardt, R. Garthoff, K. Redeker, N. Ortegel, M. Rau, and H. Weinfurter, *Phys. Rev. Lett.* **119**, 010402 (2017).

[40] X. Ma and N. Lütkenhaus, *Quantum Information & Computation* **12**, 203 (2012).

[41] E. Y.-Z. Tan, C. C.-W. Lim, and R. Renner, *Physical Review Letters* **124**, 020502 (2020).

[42] E. Woodhead, A. Acín, and S. Pironio, *Quantum* **5**, 443 (2021).

[43] P. Sekatski, J.-D. Bancal, X. Valcarce, E. Y.-Z. Tan, R. Renner, and N. Sangouard, *Quantum* **5**, 444 (2021).

[44] J. R. Gonzales-Ureta, A. Predojević, and A. Cabello, *Physical Review A* **103**, 052436 (2021).

[45] P. Brown, H. Fawzi, and O. Fawzi, *Nature communications* **12**, 1 (2021).

[46] R. Schwonnek, K. T. Goh, I. W. Primaatmaja, E. Y.-Z. Tan, R. Wolf, V. Scarani, and C. C.-W. Lim, *Nature communications* **12**, 1 (2021).

[47] G. de la Torre, J.-D. Bancal, S. Pironio, V. Scarani, *et al.*, *New Journal of Physics* **18**, 035007 (2016).

[48] D. Igor and W. Andreas, *Proc. R. Soc. Lond. A* **461**, 207 (2005).

[49] M. Navascués, S. Pironio, and A. Acín, *Phys. Rev. Lett.* **98**, 010401 (2007).

[50] S. Pironio, A. Acín, S. Massar, A. Boyer de la Giroday, D. N. Matsukevich, P. Maunz, S. Olmschenk, D. Hayes, L. Luo, T. A. Manning, and C. Monroe, *Nature* **464**, 1021 (2010).

[51] F. Dupuis, O. Fawzi, and R. Renner, *Communications in Mathematical Physics* **379**, 867 (2020).

[52] D. P. Nadlinger *et al.*, (2021), [arXiv:2109.14600](https://arxiv.org/abs/2109.14600).

[53] W. Zhang *et al.*, (2021), [arXiv:2110.00575](https://arxiv.org/abs/2110.00575).

[54] O. Nieto-Silleras, S. Pironio, and J. Silman, *New Journal of Physics* **16**, 013035 (2014).

[55] T. Cope and R. Colbeck, *Phys. Rev. A* **100**, 022114 (2019).

- [56] M. Navascués, S. Pironio, and A. Acín, *New J. Phys.* **10**, 073013 (2008).
- [57] G. Murta, S. B. van Dam, J. Ribeiro, R. Hanson, and S. Wehner, (2018), arXiv:1811.07983.
- [58] P.-S. Lin, D. Rosset, Y. Zhang, J.-D. Bancal, and Y.-C. Liang, *Phys. Rev. A* **97**, 032309 (2018).
- [59] K. Garay, J. Palfree, R. Mirin, S. W. Nam, A. U'ren, and L. K. Shalm, “Spontaneous parametric downconversion calculator,” <http://www.spdcalc.org>.
- [60] J. F. Clauser, M. A. Horne, A. Shimony, and R. A. Holt, *Phys. Rev. Lett.* **23**, 880 (1969).
- [61] S. Popescu and D. Rohrlich, *Foundations of Physics* **24**, 379 (1994).
- [62] J. Barrett, N. Linden, S. Massar, S. Pironio, S. Popescu, and D. Roberts, *Phys. Rev. A* **71**, 022101 (2005).